

A derivation of masses and total luminosities of galaxy groups and clusters in the maxBCG catalogue.

Robert N. Proctor¹, Claudia Mendes de Oliveira², Luiz Azanha², Renato Dupke^{1,3},
Roderik Overzier¹

¹ *Observatório Nacional, Rua Gal. José Cristino, 20921-400, Rio de Janeiro, Brazil*

² *Universidade de São Paulo, IAG, Rua do Matão, 1226, São Paulo, 05508-090, Brasil*

³ *University of Michigan, Ann Arbor MI 48109, USA; Eureka Scientific Inc., Oakland CA 94602-3017, USA*
email: rnp059@gmail.com

10 June 2021

ABSTRACT

We report the results of a multi-waveband analysis of the masses and luminosities of ~ 600 galaxy groups and clusters identified in the maxBCG catalogue. These data are intended to form the basis of future work on the formation of the “ m_{12} gap” in galaxy groups and clusters. We use SDSS spectroscopy and g , r and i band photometry to estimate galaxy group/cluster virial radii, masses and total luminosities. In order to establish the robustness of our results, we compare them with literature studies that utilize a variety of mass determinations techniques (dynamical, X-ray, weak lensing) and total luminosities estimated in the B , r , i , and K wavebands. We also compare our results to predictions derived from the Millennium Simulation. We find that, once selection effects are properly accounted for, excellent agreement exists between our results and the literature with the exception of a single observational study. We also find that the Millennium Simulation does an excellent job of predicting the effects of our selection criteria. Our results show that, over the mass range $\sim 10^{13} - 10^{15} M_{\odot}$, variations in the slope of the mass-luminosity scaling relation with mass detected in this and many other literature studies is in part the result of selection effects. We show that this can have serious ramifications on attempts to determine how the mass-to-light ratio of galaxy groups and cluster varies with mass.

Key words: galaxies: groups: general – galaxies: clusters: general

1 INTRODUCTION

In 1933 Fritz Zwicky applied the virial theorem to a galaxy cluster (the Coma cluster) for the first time (Zwicky 1933). He concluded that, in order to explain the cluster’s dynamics, the average density of the cluster had to be several hundred times greater than that indicated by estimates of the mass of luminous material observed in the cluster’s galaxies alone. Confirmed later in the Virgo cluster (Smith 1936), these were, of course, the first direct observations indicating the presence of dark matter (Zwicky’s “Dunkle Materie”).

Zwicky’s methodology of measuring the mass of clusters and comparing this mass to the total light emitted by the galaxies in the cluster is still in use today. Indeed, the

measurement of mass-to-light ratios in galaxy groups and clusters has become commonplace since these discoveries, as knowledge of how the mass of baryonic and non-baryonic matter are distributed within clusters provide important clues as to how they, and the galaxies within them, were formed.

However, the techniques and data involved in measuring both the masses and luminosities of clusters have become significantly more sophisticated since Zwicky’s original discovery. For instance, with the coming of large telescopes and large scale surveys, the measurement of group/cluster luminosities has advanced, permitting direct observation of galaxies further down the luminosity function and to higher

redshifts, while mass estimates can now be based upon cluster dynamics (as performed by Zwicky and Smith), or in more recent advances, X-ray properties of cluster halos or gravitational lensing. However, due to the variations in methodologies adopted in works in the literature, the received wisdom has become that it is difficult to make direct comparisons between studies.

In this work we examine this issue, comparing the results of our analysis of the masses and luminosities of ~ 600 galaxy groups and clusters identified in the maxBCG catalogue with the results of the Millennium Simulation and five other recent studies in the literature that use a variety of methodologies and data sources. Our analysis is performed in four wavebands (B , r , i and K) and includes systems of mass ranging from $\sim 10^{13}M_{\odot}$ to $10^{15}M_{\odot}$. We examine both the extensive areas of agreement, as well as areas of disagreement, between these studies and identify the issues that must be considered before making comparisons between studies.

In future papers we will use the data presented here to perform an analysis aimed at identifying the group/cluster properties driving differences in the “ m_{12} gap” (the luminosity difference between the brightest and second brightest galaxies within the central regions of groups and clusters).

Throughout this paper both our data and literature data are presented assuming a $H_0=70 \text{ km s}^{-1} \text{ Mpc}^{-1}$, $\Omega_{\Lambda}=0.7$, $\Omega_M=0.3$ cosmology. For expressing luminosities in solar units we used the values $M_{r,\odot}=4.67 \text{ mag}$, $M_{i,\odot}=4.48 \text{ mag}$, $M_{B,\odot}=5.33 \text{ mag}$, $M_{K,\odot}=3.28 \text{ mag}$.

2 DATA

Our sample was selected from groups identified in the maxBCG catalogue of Koester et al. (2007b). This catalogue was constructed from the SDSS photometric survey using a cluster finding algorithm based on three well defined properties of galaxies in clusters: spatial clustering, the presence of a “red-sequence” and the presence of a BCG (brightest cluster galaxy) at the center of the cluster (Koester et al. 2007a). Using this method Koester et al. (2007b) identify more than 13,000 clusters. Using DR9 of the SDSS-III (Ahn et al. 2012), we then selected all the clusters from the maxBCG catalogue that have a BCG with a spectroscopic redshift in the redshift interval $z = 0.05$ to $z = 0.16$ and possessing 6 or more spectroscopically confirmed members (as described in Section 2.3).

The upper end of the selected redshift range was chosen in order to ensure a substantive sample at all values of the “ m_{12} gap”, as it is necessary to probe out to redshifts of ~ 0.15 in order to obtain a reasonably large sample of the rare “fossil groups” (defined as systems with $m_{12} > 2$). The lower end of the redshift range was chosen to minimize the impact of the redshift dependent selection criteria of the SDSS spectroscopic survey which only sampled galaxies with apparent magnitude brighter than 17.7 mag in the r band, and to ensure that the peculiar velocities of the groups and

clusters studied have minimal impact on distance determinations and their associated distance moduli, and thus ensuring accurate luminosity estimates. A minimum of 6 spectroscopically confirmed members was required as the mass estimates made in this work are based on velocity dispersion estimates whose errors are large when the number of spectroscopically confirmed members is low. Indeed, even with a sample of 6 spectroscopically confirmed members, errors in $\log(\text{mass})$ estimates are of order of 0.4 dex (or a factor of 2.5 in mass).

2.1 Data from the literature

In this work we compare our results to those of five recent studies. These studies are: Girardi et al. (2002), Eke et al. (2004b), Ramella et al. (2004), Popesso et al. (2007) and Sheldon et al. (2009). These studies span four wavebands (B , r , i and K). In each case the results of these studies were, if necessary, converted to the $H_0=70 \text{ km s}^{-1} \text{ Mpc}^{-1}$, $\Omega_{\Lambda}=0.7$, $\Omega_M=0.3$ cosmology used throughout this paper. Where necessary, small corrections were also made to ensure that the same solar luminosities were used in the estimation of group/cluster luminosities and that the data are k -corrected to the same redshift ($z = 0$). We note that the literature studies above are generally based on groups/clusters at lower redshift than our data, and a minimum of 10 spectroscopically confirmed members is generally applied (rather than the 6 used here). The studies using dynamical mass estimates therefore generally possess average mass errors that are smaller than ours by, in the worst case, ~ 0.1 dex.

2.2 The Millennium Simulation

To supplement our analysis and provide a means of testing the impact on observations of errors and selection effects, we also use the galaxy recession velocities (for dynamical mass estimation) and luminosity data from the Millennium Run dark matter simulation in the WMAP1 cosmology ($H_0=73 \text{ km s}^{-1} \text{ Mpc}^{-1}$, $\Omega_{\Lambda}=0.75$, $\Omega_M=0.25$) from Springel et al. (2005), together with the semi-analytic galaxy modeling technique as described in Guo et al. (2011). The semi-analytic galaxy catalogs were converted into an observer’s light-cone geometry matched to the SDSS survey by Henriques et al. (2012) using the models of Bruzual & Charlot (2003), assuming a Chabrier (2003) initial mass function. Henriques et al. (2012) estimated total luminosities in a broad range of photometric bands from the B band to the infrared. In this work we use the r band data only. These data were converted to the $H_0=70 \text{ km s}^{-1} \text{ Mpc}^{-1}$ cosmology used throughout this paper. The corrections for Ω_{Λ} and Ω_M were deemed insignificant for this work as they cause differences of only $\sim 0.01 \text{ mag}$ and $\sim 0.4\%$ in the distance moduli and angular sizes, respectively. Data for all galaxies brighter than 22 mag in the r band (the photometric limit of the SDSS data used in our analysis) in simulated halos at redshifts less than 0.16 were obtained, and the po-

sitions and r band luminosities of each galaxy, along with the M_{200} of the parent halos, were tabulated.

2.3 Spectroscopic selection and analysis

The identification of spectroscopically confirmed cluster members was performed by an iterative procedure. First, each cluster was assumed to possess a velocity dispersion (σ) of 600 km s^{-1} . R_{200} was then estimated assuming the relation of Carlberg et al. (1997);

$$R_{200} = \frac{\sqrt{3}\sigma}{10H(z)} \text{ Mpc}. \quad (1)$$

We then searched the SDSS spectroscopic catalogue for all galaxies within the estimated R_{200} that possess redshifts differing from the BCG redshift by less than 1500 km s^{-1} (i.e. $\pm 2.5\sigma$). The value 2.5σ was selected in order to allow for the inherent scatter expected from the (almost Gaussian) distribution of velocities observed in clusters, while at the same time minimizing the likelihood of selecting interlopers. Once all the members within R_{200} were identified their redshifts were used to calculate a new velocity dispersion using the Beers et al. (1990) bi-weight estimator for systems with more than 10 members, and the Beers et al. (1990) gapper method for systems with 10 or less members. For cases where the initial velocity dispersions were an underestimate this resulted in an increase in the velocity dispersion (and hence R_{200}) estimate, as well as increasing the permitted velocity range ($\pm 2.5\sigma_{\text{new}}$). Conversely, for systems in which the initial values were an overestimate the new values were lower. This process was iterated a number of times. We found that, generally, convergence was achieved after only two or three iterations. However a total of 10 iterations were performed. This permitted the use of the value from the last (10th) iteration as the final result for each group/cluster, while the RMS scatter in the last 6 iterations was taken as an additional uncertainty in the velocity dispersion and which was added in quadrature to the formal velocity dispersion error. We note that this additional error is zero for the majority of systems in which the procedure converged.

At this stage, groups/clusters with less than 6 spectroscopically confirmed members within R_{200} were discarded from the sample. Clusters for which the average recession velocity of all the galaxies *except* the BCG differed from the recession velocity of the BCG by more than 400 km s^{-1} were also excluded, as these have a high probability of being either highly disturbed (i.e. non-virialized) systems or false/contaminated detections due to line-of-sight effects.

2.4 Mass estimation

The masses of the remaining maxBCG clusters were estimated using:

$$M_{200} = \frac{3}{G}\sigma_{200}^2 R_{200}. \quad (2)$$

This equation can be reformulated using Equation 1 to give a more convenient form:

$$\log(M_{200}) = 3\log(\sigma_{200}) + 6.24 - \log(E(z)), \quad (3)$$

where, for a flat Universe:

$$E(z) = \sqrt{\Omega_M(1+z)^3 + \Omega_\Lambda}. \quad (4)$$

However, it is helpful to note that $\log(E(z))$ is small (~ 0.02 at the $z = 0.1$ median of the data presented here) and varies by only ± 0.02 over the whole redshift range of the clusters reported here. The resultant masses spanned the range from $\sim 10^{13}$ to $\sim 10^{15} M_\odot$.

We note that four of the five literature studies to which we compare our results (Girardi et al. 2002; Eke et al. 2004b; Ramella et al. 2004; Popesso et al. 2007) use Equation 2 to estimate masses. However, both Girardi et al. (2002) and Popesso et al. (2007) make corrections for a surface pressure term. A comparison of the masses presented in Girardi et al. (2002) with masses estimated using their velocity dispersions and Equation 2 yields an offset of 0.00 dex with RMS scatter of only 0.12 dex. This demonstrates that this term is small and of no significance to the results presented here. Eke et al. (2004b), on the other hand, use the spatial distribution of the galaxies in each system to estimate R_{200} rather than Equation 1, basing their values of radius on a calibration against cosmological simulations (Eke et al. 2004a)¹. Finally, (Sheldon et al. 2009) utilize SDSS i band photometry and masses derived from weak gravitational lensing.

As a first test of our dynamical mass estimates, we performed a search of the literature for groups/clusters in our study for which masses derived from X-ray properties have either been reported or can be estimated. A total of 24 groups from our study were found to have masses based on a variety of X-ray properties reported in the literature (Donahue et al. 2005; Jia, Chen & Chen 2006; Lemze et al. 2008; Zibetti, Pierini & Pratt 2009; Akamatsu et al. 2011; Proctor et al. 2011; Miller et al. 2012; Owers et al. 2014). For the majority of of these studies (Donahue et al. 2005; Zibetti, Pierini & Pratt 2009; Akamatsu et al. 2011; Proctor et al. 2011; Miller et al. 2012; Owers et al. 2014) X-ray masses were estimated from X-ray temperature using the the Tier 1 relation from Sun et al. (2009) (their Table 6). However, the X-ray masses taken from Jia, Chen & Chen (2006) were deived using X-ray temperature and electron density, while in the case of Lemze et al. (2008), weak lensing and the X-ray luminosity profile were employed to determine cluster masses. The masses derived from all the above studies assume hydrostatic equilibrium.

¹ N.B. We have converted the b_j given in Eke et al. (2004b) to the B band using the relation $L_{bj} = 1.1L_B$ given by their Equation 4.3

The results of the comparison of dynamical masses to those derived from X-ray data are shown as solid points in Fig. 1. Also shown in this figure as open squares are total cluster masses derived from Zhang et al. (2011) X-ray gas masses assuming the relation derived by Mahdavi et al. (2013) between X-ray gas masses and total cluster masses. This relation was calibrated by comparing gas masses from X-ray analyses to the results of total cluster masses from weak lensing. Dynamical masses for these data were derived using the velocity dispersions provided in Zhang et al. (2011) and Equation 3. Velocity dispersions and masses derived from X-ray temperature were also taken from Osmond & Ponman (2004) and Wu, Xue & Fang (1999). For these data, dynamical masses were derived using Equation 3, while X-ray masses were derived from the X-ray temperatures using Sun et al. (2009) as above. The results of Osmond & Ponman (2004) and Wu, Xue & Fang (1999) are shown in Fig. 1 as open circles and triangles respectively. Again, hydrostatic equilibrium is assumed in all cases, and all the above results are for masses within R_{200} . Where necessary, we assumed $R_{200}=1.54R_{500}$, consistent with the values of R_{200} and R_{500} for clusters given in Ettori et al. (2010), yielding $M_{200}=1.46M_{500}$.

Now, given the inhomogeneity of these data, and the need to convert between M_{500} and M_{200} , it would be unwise to over-interpret this plot. However, we note that in Fig. 1, systems with masses above $\sim 10^{14} M_{\odot}$, although running parallel to the one-to-one line, the X-ray masses appear systematically offset from the dynamical masses by ~ 0.15 dex. On the other hand, the systems with masses lower than $\sim 10^{14} M_{\odot}$ (which are from Osmond & Ponman (2004)), the data straddle the one-to-one line, but appear to exhibit a slope greater than one. This change in gradient at low masses was noted in Osmond & Ponman (2004) when they considered their $L_X - \sigma$ and $\sigma - T_X$ plots (their Sections 7.2 and 7.3) and was also noted in Helsdon & Ponman (2000). A break in the slope of the X-ray scaling relations at a temperature of about 1 keV (corresponding to a mass of $\sim 10^{14} M_{\odot}$) is also evident in a number of studies (e.g. Xue & Wu (2000) and Harrison et al. (2012)). However, it has been disputed in other works, e.g. Mulchaey (2000). Therefore, there remains no real consensus as to whether the apparent change in gradient in the $L_X - \sigma$ and $\sigma - T_X$ scaling relations represents a true physical effect or is rather an artifact of large errors and selection effects in low mass systems (see Osmond & Ponman (2004) for a more detailed description of the controversy).

It is also interesting to perform a similar comparison using the Millennium Simulation data, in this case comparing dynamical mass to the M_{200} values given in the database. The masses presented in the database were calculated by simply adding the masses of all the particles within the region of each halo where the average density is 200 times the critical density. In order to calculate dynamical masses we applied the same analysis as that applied to our observational data. i.e. assuming that the brightest cluster galaxy lay at the center of the cluster and measuring re-

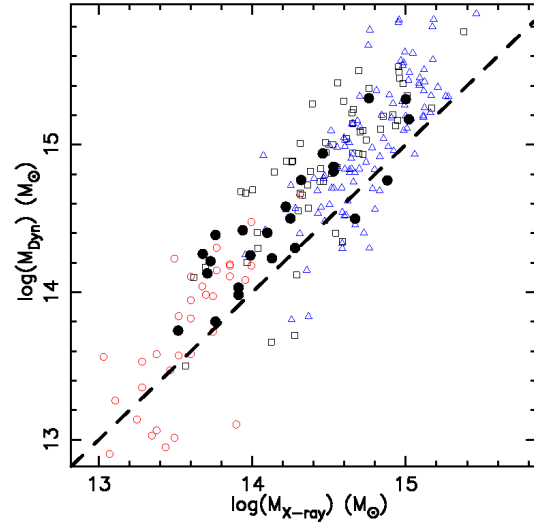


Figure 1. Comparison of dynamical mass, estimated as detailed in the text, with masses derived from X-ray data. Black dots are clusters in our study (whose dynamical masses are estimated here) with X-ray masses from the literature. Open squares are derived from the velocity dispersion and X-ray gas mass data from Zhang et al. (2011) (see text). Open circles and triangles are derived from the velocity dispersion and X-ray temperature data of Osmond & Ponman (2004) and Wu, Xue & Fang (1999), respectively. The dashed line shows the one-to-one locus. At masses greater than $\sim 10^{14} M_{\odot}$ there is a clear, constant offset between X-ray and dynamical masses, while below this mass there is a suggestion of a change in slope in the correlation.

cession velocities with respect to the central galaxy using the Beers et al. (1990) bi-weight and gapper estimators as described in Section 2.3 to estimate velocity dispersion. Dynamical masses are then estimated using Equation 3. This analysis was performed under the assumption of a variety of selection criteria, including those describing our observational data, which we recall were selected to have redshifts between 0.05 and 0.16, and have 6 or more members with apparent magnitudes brighter than the 17.7 mag within R_{200} . For each analysis, the median of the dynamical mass data in bins of Millennium Simulation mass were calculated. We note that our use of the median in these analyses ensures that the effects of the asymmetrical errors in dynamical mass are essentially eliminated.

The comparison between Millennium Simulation masses and dynamical masses is shown in Fig. 2. In this plot the dynamical masses are those for all systems with a minimum of 6 members, but with no redshift or member luminosity selection limits applied. Reasonable agreement is found. At masses greater than $\sim 10^{14} M_{\odot}$ the Millennium Simulation masses show an offset from the median dynamical masses of ~ 0.1 dex, similar to the trend in the X-ray data in Fig. 1. Below $\sim 10^{14} M_{\odot}$, the correlation between M_{MS} and M_{Dyn} steepens, with the gradient increasing from 1.05 above $\sim 10^{14} M_{\odot}$ to 1.17 below this mass. Although statis-

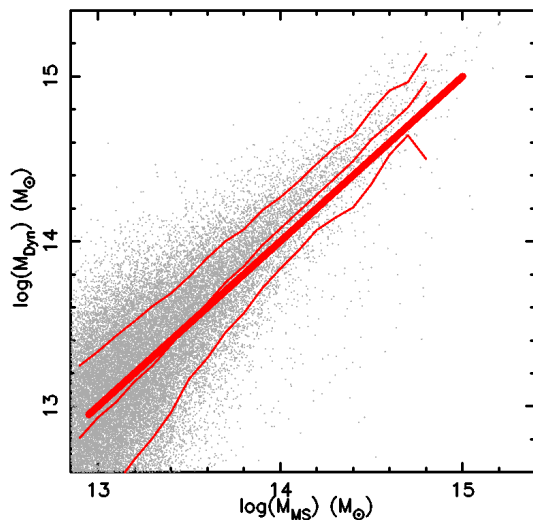


Figure 2. Comparison of masses using our dynamical mass estimation method (see text) with masses from the Millennium Simulation. The thick red line shows the one-to-one locus, while the thin lines show the median and 15/85 percentiles of the dynamical masses in bins of 0.1 dex in Millennium Simulation mass. As well as an offset at high masses, the data exhibit an increase in slope at masses below $10^{14} M_{\odot}$.

tically only marginally ($\sim 2\sigma$) significant, this steepening at low masses is again at least qualitatively similar to the X-ray data. Some care must be taken in the interpretation of these differences, since given the large uncertainties in the semi-analytic models that describe the baryonic physics, there is no guarantee that the Millennium Simulation data match the real Universe in this regard. However, it is interesting to note that offset at high masses and the increased gradient at lower masses are at least qualitatively consistent with the trends in the X-ray data. This therefore raises the possibility that this represents a real systematic bias in dynamical masses, perhaps due to a bias in the distribution of galaxies with respect to the underlying dark matter halo or perhaps representing a breakdown in the assumptions made in deriving dynamical masses (i.e. the assumption of full virialization and/or that the systems are well described as isothermal spheres).

2.5 Photometric analysis

Having established estimates of the masses of the clusters in our sample we must next estimate the total luminosity of each of the systems. Therefore, for each of the clusters selected above, the g , r and i band photometry of all galaxies within $4R_{200}$ of the BCG were obtained from the SDSS photometric survey. We use the SDSS model magnitudes which were estimated using a combination of De Vaucouleurs and exponential profiles. Galaxies with SDSS spectroscopic redshifts were k-corrected to zero redshift using the colour dependent functions of Chilingarian et al. (2010).

For each cluster, and in each waveband (g , r and i), the total luminosity of the galaxies within R_{200} was then estimated in a two step process. First, the luminosities of all the spectroscopically confirmed galaxies within R_{200} of each group were co-added to derive the total luminosity. Next, the total luminosity of all galaxies in the photometric survey with apparent magnitudes fainter than 17.7 mag in the r band (the lower limit of the spectroscopic survey) and brighter than 22.2 mag (the 95% completeness limit of the photometric survey) were co-added. We note that modeling of the Blanton et al. (2003) SDSS r band luminosity function indicates that even in our most distant clusters the contribution to the total light of galaxies fainter than our upper limit of 22.2 would be less than 2.5% (i.e a $\log(\text{luminosity})=0.01$). This contribution is therefore deemed insignificant to our results, and is ignored.

A colour cut excluding all galaxies 0.2 mag redder in $(g-r)$ than the BCG was applied in order to minimize the impact of contamination by high redshift interlopers. In order to estimate the background contamination, the same process was applied to seven concentric annuli between $3R_{200}$ and $4R_{200}$. These annuli were selected to have an area equal to the area of the central region within R_{200} . In each of the g , r and i bands the median value of the seven annuli was then taken as the background level and this value was subtracted from the value calculated within R_{200} yielding an estimate of the total luminosity of faint galaxies within R_{200} . These luminosities were also then k-corrected to zero redshift using the functions of Chilingarian et al. (2010). The total luminosity in faint galaxies was then added to the total luminosity in spectroscopically confirmed galaxies to yield a total luminosity for each group.

However, in some cases the background luminosity in faint galaxies exceeded the estimated total luminosity of *all* the galaxies in the cluster, resulting in negative values for the luminosity of the cluster, clearly indicating that the background level was overestimated. Such clusters were excluded from our analysis. In other cases, despite high background levels, the total luminosities of the clusters remained positive raising the possibility that the clusters had, indeed, very low luminosity compared to the background against which they are projected. In such cases we excluded only clusters in which the background level exceeded five times the luminosity of faint galaxies in the cluster, deeming the uncertainties in the background level to be too large for a reliable total luminosity estimate.

After all the selection cuts above were made we retained a total of 614 clusters.

In order to compare literature values in the B and K bands we used the colour dependent functions of Blanton & Roweis (2007) (B band) and Yaz et al. (2010) (K band) to estimate the luminosities of each galaxy in each cluster in these bands. The total luminosities in the bands were then also estimated as above.

3 RESULTS

In this section we report our results and compare them to five recent works from the literature that measure masses and luminosity ratios in significant samples of groups/clusters in the B , r , i and K bands (recall that, for our results, r and i are taken directly from the SDSS database while B and K are generated from the SDSS data using the colour dependent transforms of Blanton & Roweis (2007) and Yaz et al. (2010) respectively). A full table of results is available from the authors and will be made available on-line.

Fig 3 shows mass against luminosity for the clusters in our final sample in all four bands (436, 614, 611 and 427 clusters in B , r , i and K bands, respectively). Lines of constant log of the mass-to-light ratio ($[M/L]=\log(M/M_\odot)-\log(L/L_\odot)$) are shown for $[M/L]=3.0, 2.5, 2.0$ and 1.5 (decreasing to the lower right).

In the figure our data are shown as black points, while in each panel, data from the literature are also presented as either red points (when actual data are available) or red lines (when the literature provide fits to data). Note that in all cases the literature data have been converted (when necessary) to a $H_0=70 \text{ km s}^{-1} \text{ Mpc}^{-1}$, $\Omega_\Lambda=0.7$ cosmology, k -corrected to $z = 0$ and adjusted the solar luminosities given in the introduction.

Fig. 3 generally shows good agreement between our data and the literature studies shown in red, particularly at masses higher than $>10^{14} M_\odot$. However, there appear to be two areas of poorer agreement - the first in the comparison to the study of Girardi et al. (2002), and the other at the low mass end of our mass range (i.e. $<10^{14} M_\odot$) in the B , r and i bands.

Addressing first the poor agreement with the study of Girardi et al. (2002) in the B band, there is clearly an offset between our data and the results of Girardi et al. (2002) at higher masses ($>10^{14} M_\odot$), with the average of $\log(L)$ within ± 0.1 dex of $\log(M) = 14.25$ being 11.67 and 11.97 for our and Girardi et al. (2002) data respectively - i.e. a 0.3 dex (or factor of 2) difference in luminosity at a given mass, and therefore in the mass-to-light ratio. However, we note that our results *are* consistent with the study of Eke et al (2004b) in the B band, as well as with the studies of Popesso et al. (2007), Sheldon et al. (2009), Ramella et al. (2004) in the r , i and K bands respectively. We then conclude that the Girardi et al. (2002) study suffers from an, as yet unidentified, systematic difference in their luminosity estimates with respect to other recent studies. We assume the offset to be in the luminosity direction because, as noted in Section 2.4, we have already shown that the mass estimation methodology of Girardi et al. (2002) is completely consistent with the simple dynamical mass estimates made in this paper.

Turning our attention to the disparities at low masses, our results clearly show a pronounced increase in the slope of the mass-luminosity relation as we go to low masses. However, we note that many of the literature studies presented in Fig. 3 appear to show similar, albeit smaller, increases

in the slope of the mass-luminosity relation at the low mass end. The effect is clearly seen in the studies of Girardi et al. (2002), Eke et al. (2004b) and can also be seen in the data of Sheldon et al. (2009) in which the gradient decreases from ~ 1.6 below $10^{14} M_\odot$ to ~ 1.3 above this mass. The power-law fits of Popesso et al. (2007) or Ramella et al. (2004) do not, perforce, exhibit such gradient changes. However, in the case of Ramella et al. (2004), the study contains very few points at the low masses of interest here, while the Popesso et al. (2007) study presents data selected from two catalogues, one optical, the other an X-ray catalogue. Examination of Fig. 9 of Popesso et al. (2007) shows that the optically selected sample *does* exhibit an increase in the slope of the mass-luminosity relation at the lowest masses, while the X-ray selected systems do not. This suggests that this trend may be, at least in part, the result of optical selection effects (a point that was also raised in the recent paper of Mulroy et al. (2014)). In fact, our study, which requires at least 6 bright galaxies within R_{200} of galaxies in the redshift range $z = 0.05$ to $z = 0.16$, is generally biased towards higher redshifts than the other studies which are dominated by much closer systems. This raises the possibility that this optical selection effect may be playing a stronger role shaping the locus of our results than in the other studies presented here. To examine this possibility in more detail we again turn to the Millennium Simulation.

In Fig. 4 we show the mass-luminosity relation for groups and clusters in the Millennium Simulation. The medians of the dynamical mass data in bins of luminosity are shown as solid red lines. The 15th and 85th percentiles are shown as dashed lines. In the top panel we plot the masses and luminosities taken directly from the simulation. In the bottom two panels we plot dynamical masses derived from the simulation (see Section 2.2). In the top and middle plots all groups and clusters with 6 or more member galaxies (irrespective of their luminosities or redshifts) are plotted. In the bottom panel we apply the SDSS selection criteria - i.e. 6 or more galaxies brighter than 17.7 mag in the r band, and redshifts in the range $0.05 < z < 0.16$. The bottom panel therefore represents the Millennium Simulation prediction for the locus of our observational data.

Comparing first the top two panels, the displacement and non-linearity in the relation between Millennium Simulation mass and dynamical mass identified in Fig. 2 is also evident when comparing these two plots. A marked increase in scatter is also clearly seen in the dynamical mass data.

Comparison of the bottom two panels shows the effect of requiring 6 or more bright members ($r < 17.7$ mag) within R_{200} and restricting the redshift range to $0.05 < z < 0.16$. Clearly, at low masses, when combined with the requirement of a minimum number of bright members for dynamical analysis, this redshift restriction causes only the brightest groups and clusters at any given mass to be selected, thus introducing another strong non-linearity into the apparent mass-luminosity relation. What is more, comparison of the bottom plot with the r band data in Fig. 3 suggests that

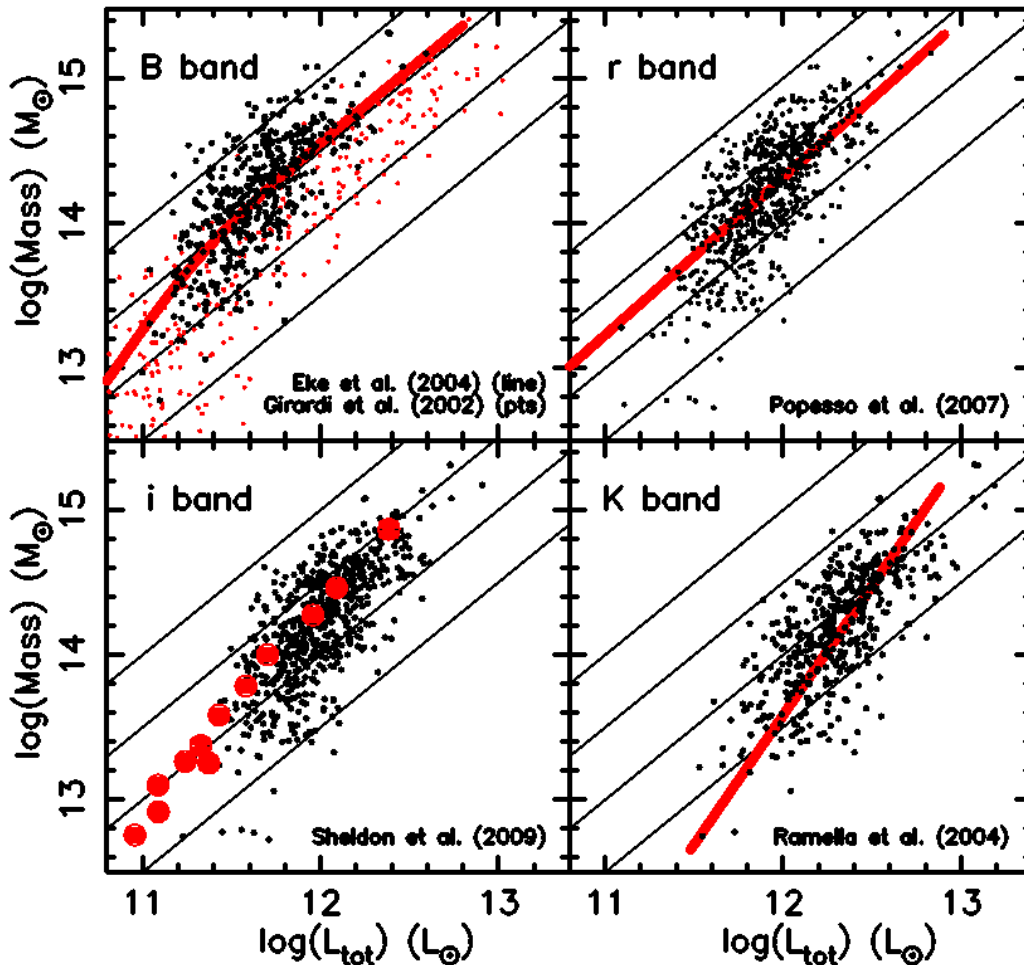


Figure 3. Mass is plotted against total group/cluster luminosity. Black dots are our data, while red points and lines are taken from literature studies (as detailed in the bottom right of each panel). The four black lines in each panel are lines of constant log of the mass-to-light ratio ($[M/L]$), with values of 3.0, 2.5, 2.0 and 1.5, decreasing from upper left to the lower right. Agreement between our data and literature data is generally good at high masses, but at lower masses and in the comparison to Girardi et al. (2002) in the B band discrepancies are evident.

Table 1. The offsets from the median of the 15th and 85th percentiles in three masses bins in both our data and the Millennium Simulation (MS).

$\log(M) (M_{\odot})$	Data		MS	
	15%	85%	15%	85%
13.3	-0.52	0.39	-0.50	0.45
14.0	-0.32	0.30	-0.39	0.33
14.7	-0.27	0.27	-0.28	0.25

the Millennium Simulation is reproducing the observational data extremely well.

In order to demonstrate this, in Fig. 5 we plot the predictions of the simulation for the mass-to-light ratio against mass scaling relation and compare to the medians of the observational data and their uncertainties. We choose to show

mass-to-light ratio here as the relatively small dynamical range of this parameter serves to emphasize similarities and differences between the various data sets, while the binning of the data has significantly reduced the correlated errors which would otherwise make interpretation of such a plot difficult.

In Fig. 5 the data taken directly from the Millennium Simulation is shown as a thick solid line. For ease of comparison, this line has been shifted by the ~ 0.1 dex offset between Millennium Simulation and dynamical masses first identified in Fig. 2 and also evident in Fig. 4. The data for dynamical masses with no luminosity or redshift selection criteria applied is shown as a thin solid line, while the dynamical mass data with luminosity and redshift selection criteria applied is shown as a dashed line.

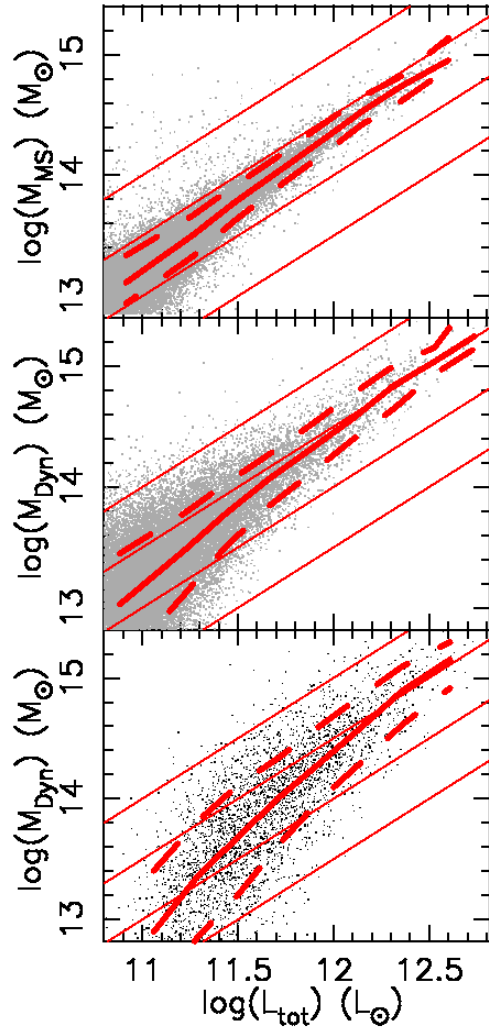


Figure 4. The r band mass-luminosity relation of groups/clusters in the Millennium Simulation. In the top panel Millennium Simulation mass (rather than dynamical mass) is plotted, while the bottom two panels show dynamical mass. In the top two panels all systems with redshift less than 0.16 are shown, while in the bottom panel our observational selection criterion of a minimum of 6 bright galaxies within R_{200} of systems at $0.05 < z < 0.16$ is applied. Solid and dashed red lines are the median with 15th and 85th percentiles, respectively.

The changing slope in the Millennium Simulation mass against dynamical masses relation noted in Fig. 2 at $\sim 10^{14} M_{\odot}$ is again evident in this plot, with the two solid lines exhibiting the same shallow slope above this mass, but steepening and diverging below. Examination of Fig. 5 also shows that the Millennium Simulation prediction for the locus of mass-to-light ratio against mass relation for data using dynamical masses and with selection criteria applied (dashed line) is an extremely good match to the observational data.

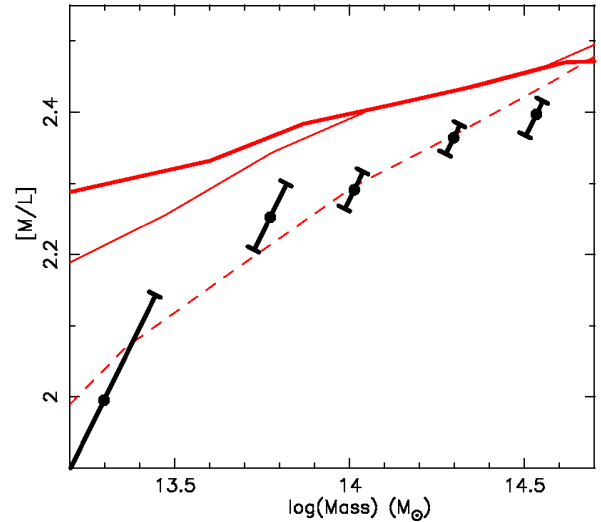


Figure 5. Mass-to-light ratio in the r band are plotted against against mass. The medians of observational data and their (correlated) uncertainties are shown as black points with error bars. Millennium Simulation data are shown as red lines. Data taken directly from the Millennium Simulation are shown a thick solid line, while the data for dynamical masses derived from the simulation with no selection criteria applied (see text) are shown a thin red line. The data from the simulation using dynamical mass and with selection criteria applied is shown as a dashed line. The simulation clearly reproduces the observational data extremely well.

What is more, in Table 1 we show the width of the 15th and 85th percentiles in dynamical mass at selected points along the mass-luminosity relations of the simulated and real data, and agreement is again excellent. Clearly, the Millennium Simulation is doing a remarkably good job of reproducing the actual observational data.

Our analysis of the Millennium Simulation has therefore clearly identified the importance of selection effects in shaping the locus of the mass-luminosity relation found from our data, and suggests that such effects may be present to, some lesser extent, in the other studies considered here. Indeed, the excellent agreement found between our data and the Millennium Simulation suggest that the simulation might be used to identify, and even correct for, such effects in future studies.

4 CONCLUSIONS

As the first step in a program to perform a detailed study of “fossil groups”, we have estimated masses and total luminosities in ~ 600 groups and clusters identified in the maxBCG catalogue using SDSS photometry and spectroscopy. We have also performed an analysis of Millennium Simulation data subjected to the same processes and selection criteria as the observational data. We have compared our results with five other studies in the literature in four

different wavebands (B , r , i and K) and the Millennium Simulation data.

At high masses ($>10^{14} M_{\odot}$) we find extremely good agreement with four of the five literature and the Millennium Simulation results, but find an exception in a single literature study (Girardi et al. 2002), which appears discordant. At lower masses the agreement of our data with literature results is poorer. However, we have used the Millennium Simulation to demonstrate that a large part of the discrepancies at these masses can be explained by selection effects.

We have also used the Millennium Simulation to provide a hint to the cause of remaining discrepancies at lower mass, showing that within the simulation the assumption that mass is proportional to σ^3 begins to fail as one approaches lower masses. With hints of a similar phenomena already having been observed in X-ray data (e.g. Helsdon & Ponman 2000; Osmond & Ponman 2004), this is an issue that certainly warrants further investigation. It should be noted that our findings with regard the Millennium Simulation are of particular importance in studies that attempt to measure the gradient of the mass-to-light ratio against mass scaling relation which, as is evident from our results, are extremely susceptible to these effects.

REFERENCES

- Ahn et al., 2012, ApJS, 203, 21
 Akamatsu H., Hoshino A., Ishisaki Y., Ohashi T., Sato K., Takei Y., Ota N., 2011, PASJ, 63, 1019
 Beers T.C., Flynn K., Gebhardt K., 1990, AJ, 100, 32
 Blanton et al., 2003, ApJ 592, 819
 Blanton M.R., Roweis S.T., 2007, AJ, 133, 734
 Bruzual, G., Charlot S., 2003, MNRAS, 344, 1000
 Carlberg et al., 1997, ApJ, 485, 13
 Chabrier G., 2003, PASP, 115, 763
 Chilingarian I., Melchior A-L., Zolotukhin I.Y., 2010, MNRAS, 405, 1409
 Donahue M., Voit G.M., O’Dea C.P., Baum S.A., Sparks W.B., 2005, ApJ, 630, 13
 Eke et al., 2004a, MNRAS, 348, 866
 Eke et al., 2004b, MNRAS, 355, 769
 Ettori S., Gastaldello F., Leccardi A., Molendi S., Rossetti M., Buote D., Meneghetti M., 2010, A&A, 524, 68
 Girardi M., Manzato P., Mezzetti M., Giuricin G., Limboz., 2002, ApJ, 569, 720
 Guo et al. 2011, MNRAS, 413, 101
 Harrison et al., 2012 ApJ, 752, 12
 Helsdon S.F., Ponman, T. J., 2000 MNRAS, 315, 356
 Henriques et al., 2012, MNRAS, 421, 2904
 Jia S. M., Chen Y., Chen L., 2006, ChJAA, 6, 181
 Koester et al., 2007a, ApJ, 660, 221
 Koester et al., 2007b, ApJ, 660, 239
 Lemze D., Barkana R., Broadhurst T.J., Rephaeli Y., 2008, MNRAS, 386, 1092
 Mahdavi A., Hoekstra H., Babul A., Bildfell C., Jeltama T., Henry J.P., 2013, AJ, 767, 116
 Miller et al., 2012, ApJ, 747, 94
 Mulchaey J.S., 2000, ASP Conference Series, Vol. 209, 2000
 Muiyroy et al., 2014, MNRAS, 443, 3309
 Osmond J. P. F., Ponman T. J., 2004, MNRAS, 350, 1511
 Owers et al., 2014, ApJ, 780, 163
 Popesso P., Biviano A., Bohringer H., Romaniello M., 2007, A&A, 464, 451
 Proctor R., Mendes de Oliveira C., Dupke R., Lopes de Oliveira R., Cypriano E.S., Miller E., Rykoff E., 2011, MNRAS 418, 2054
 Ramella M., Boshin W., Geller M.J., Mahdavi A., Rines K., 2004, AJ, 128, 2022
 Sheldon et al., 2009, AJ, 703, 2232
 Smith, S 1936, ApJ, 83, 23
 Springel et al., 2005, Nature, 435, 629
 Sun M., Voit G.M., Donahue M., Jones C., Forman W., Vikhlinin A., 2009 ApJ, 693, 1142
 Wu X.-P., Xue Y.-J., Fang L.-Z., 1999, ApJ, 524, 22
 Xue Y.-J., Wu X.-P 2000 ApJ, 538, 65
 Yaz E., Bilir S., Karaali S., Ak S., Coşkunoglu B., Cabrera-Lavers A., 2010, Astron. Nachr., 331, 807
 Zhang Y.-Y., Andernach H., Caretta C.A., Reiprich T.H., Bohringer H., Puchwein E., Sijacki D., Giradi M., 2011, A&A, 526, 105
 Zibetti S., Pierini D., Pratt G.W., 2009, MNRAS, 392, 525
 Zwicky F., 1933, Helv. Phys. Acta, 6, 110

Acknowledgments

The authors would like to thank Eduardo Cypriano for many useful discussions. CMDO acknowledges support from FAPESP (grant number 2006/56213-9) and CNPq. LA acknowledges support from a CNPq PIBIC fellowship. The Millennium Simulation databases used in this paper and the web application providing online access to them were constructed as part of the activities of the German Astrophysical Virtual Observatory (GAVO). Funding for SDSS-III has been provided by the Alfred P. Sloan Foundation, the Participating Institutions, the National Science Foundation, and the U.S. Department of Energy Office of Science. The SDSS-III web site is <http://www.sdss3.org/>. SDSS-III is managed by the Astrophysical Research Consortium for the Participating Institutions of the SDSS-III Collaboration including the University of Arizona, the Brazilian Participation Group, Brookhaven National Laboratory, Carnegie Mellon University, University of Florida, the French Participation Group, the German Participation Group, Harvard University, the Instituto de Astrofísica de Canarias, the Michigan State/Notre Dame/JINA Participation Group, Johns Hopkins University, Lawrence Berkeley National Laboratory, Max Planck Institute for Astrophysics, Max Planck Institute for Extraterrestrial Physics, New Mexico State University, New York University, Ohio State University, Pennsylvania State University, University of Portsmouth, Princeton University, the Spanish Participation Group, University of

Tokyo, University of Utah, Vanderbilt University, University of Virginia, University of Washington, and Yale University.